Characterization of Starch Polymorphic Structures Using Vibrational Sum Frequency Generation Spectroscopy

Lingyan Kong – Pennsylvania State University

Christopher Lee – Pennsylvania State University

Seong H. Kim – Pennsylvania State University

Gregory R. Ziegler – Pennsylvania State University

Citation of published version:
Kong, L., Lee, C., Kim, S., Ziegler, G. (2014): Characterization of Starch Polymorphic Structures Using Vibrational Sum Frequency Generation Spectroscopy. *The Journal of Physical Chemistry B*, 118(7).

DOI: https://doi.org/10.1021/jp411130n

THE JOURNAL OF PHYSICAL CHEMISTRY B

Article

pubs.acs.org/JPCB

Characterization of Starch Polymorphic Structures Using Vibrational Sum Frequency Generation Spectroscopy

Lingyan Kong,[†] Christopher Lee,[‡] Seong H. Kim,*[,‡,§] and Gregory R. Ziegler*[,†,§]

[†]Department of Food Science, Pennsylvania State University, University Park, Pennsylvania 16802, United States

[‡]Department of Chemical Engineering, Pennsylvania State University, University Park, Pennsylvania 16802, United States

[§]Materials Research Institute, Pennsylvania State University, University Park, Pennsylvania 16802, United States

Supporting Information

ABSTRACT: The polymorphic structures of starch were characterized with vibrational sum frequency generation (SFG) spectroscopy. The noncentrosymmetry requirement of SFG spectroscopy allows for the detection of the ordered domains without spectral interferences from the amorphous phase and also the distinction of the symmetric elements among crystalline polymorphs. The V-type amylose was SFG-inactive due to the antiparallel packing of single helices in crystal unit cells, whereas the A- and B-type starches showed strong SFG peaks at 2904 cm^{-1} and 2952−2968 cm^{-1}, which were assigned to CH stretching of the axial methine group in the ring and CH_2 stretching of the exocyclic CH_2OH side group, respectively. The CH_2/CH intensity ratios of the A- and B-type starches are significantly different, indicating that the conformation of hydroxymethyl groups in these two polymorphs may be different. Cyclodextrin inclusion complexes were also analyzed as a comparison to the V-type amylose and showed that the head-to-tail and head-to-head stacking patterns of cyclodextrin molecules govern their SFG signals and peak positions. Although the molecular packing is different between V-type amylose and cyclodextrin inclusion complexes, both crystals show the annihilation of SFG signals when the functional group dipoles are arranged pointing in opposite directions.

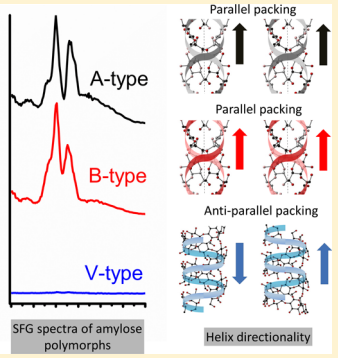

INTRODUCTION

Starch is among the most abundant natural polymers on earth and is the primary form of energy storage in plants. In addition to providing the majority of calories in human diets, starches and modified starches find numerous food and nonfood applications. Native starch occurs in the form of granules that have complex semicrystalline and hierarchical structures.[1] In plants, starch mainly consists of two structurally distinct homopolymers: amylose and amylopectin. Amylose is a linear or lightly branched polymer of (1→4)-linked α-glucopyranose, while amylopectin is a highly branched polymer of (1→4)-linked α-glucopyranose with α-(1→6) branch linkages. The ratio of the two component homopolymers in starches varies with their botanical origin.

The crystallization of amylose and amylopectin gives rise to different polymorphic structures as revealed in X-ray diffraction (XRD) patterns. Amylopectin can exist in two different polymorphic forms, i.e., A-type, mainly from cereal starches (e.g., corn, wheat), and B-type, typical of tuber starches (e.g., potato) and high amylose starches (e.g., high amylose maize starch).[2] Amylose is not usually crystalline in its native state, but it can be recrystallized in vitro into the V-type structure through association with guest molecules.[3]

Different structural models of crystalline starch polymorphs have been proposed. The most widely accepted or discussed models are schematically shown in Figure 1. Both the A and B structures are thought to be composed of left-handed, parallel-stranded double helices packed parallel in the crystalline lattice (Figure 1a and 1b).[4−7] The two polymorphs differ in their packing of double helices and number of water molecules within the crystalline lattice.[4−7] According to Imberty et al.,[4] the A-type polymorph has a monoclinic unit structure, where unit cell parameters are a = 21.24 Å, b = 11.72 Å, c = 10.69 Å, and $\alpha = \beta = 90°$, $\gamma = 123.5°$. It contains two double helices and four water molecules per unit cell (one water molecule per glucosyl unit). Popov et al.[6] recently succeeded in growing A-amylose crystals larger than 10 μm and used a microfocused synchrotron X-ray source to obtain higher resolution diffraction data. Although their data confirmed the overall features of the previous model of this polymorph, some fine details had to be modified. Their new model contained two intracrystalline water molecules per glucosyl unit, instead of one in the previous model. There are three possible $C6H_2OH$ conformations (Figure 1d), and in the new model the hydroxymethyl groups of each glucosyl residue adopt the *gg* conformation. According to Imberty et al.[5] and Takahashi et al.,[7] the B-type was modeled as a hexagonal unit structure with approximate unit cell parameters, $a = b$ = 18.5 Å, c = 10.4 Å, and $\alpha = \beta = 90°$, $\gamma = 120°$, containing two double helices and 36 water molecules per unit cell. The hydroxymethyl groups also adopt the *gg* conformation. In addition, the A and B structures differ in the symmetry of the double helices.[8] The A type has a

Received: November 12, 2013
Revised: January 14, 2014
Published: January 16, 2014

   dx.doi.org/10.1021/jp411130n | J. Phys. Chem. B 2014, 118, 1775−1783

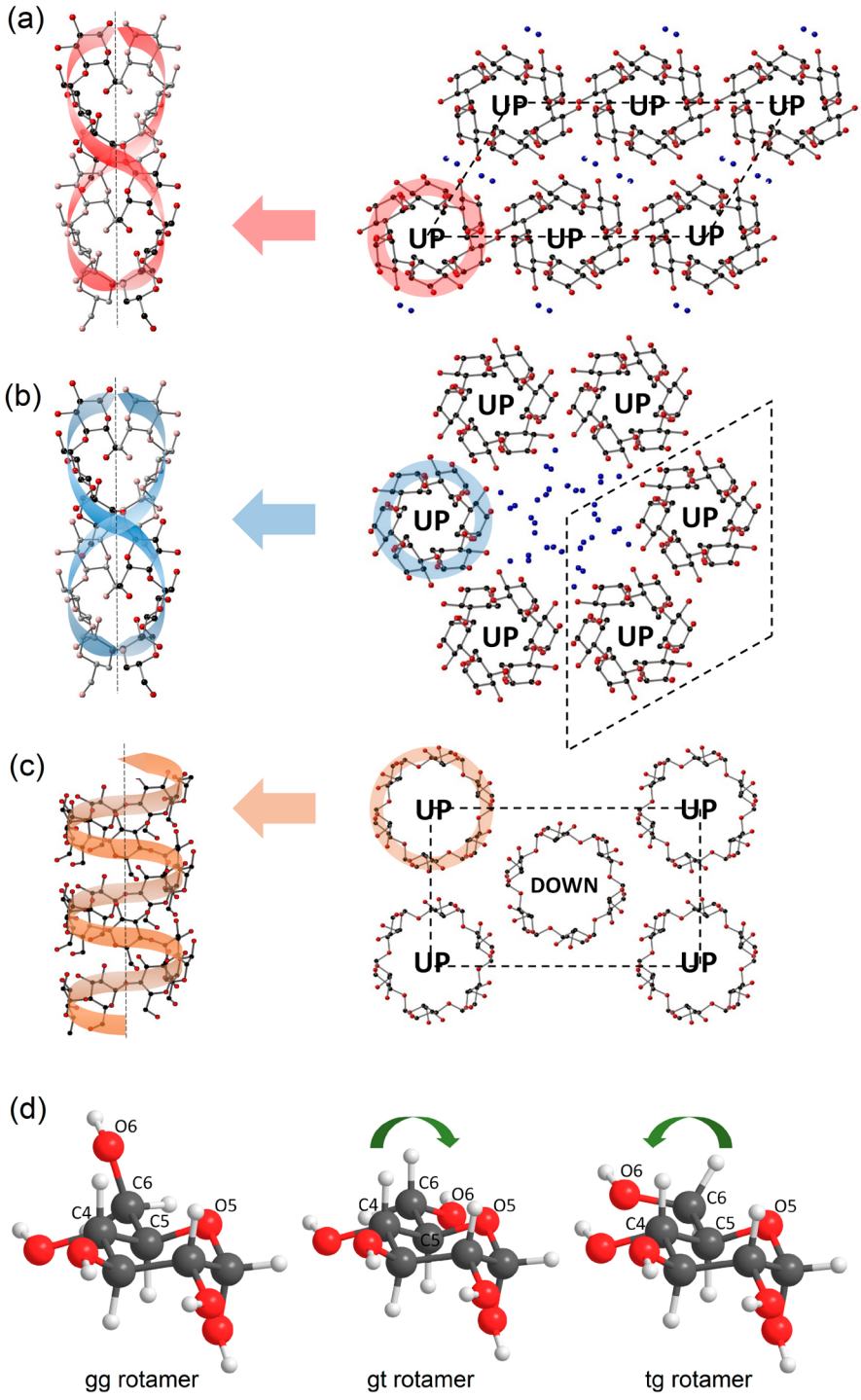

Figure 1. Molecular models of helices (left) and *c*-axis unit cell projections (right) of (a) A-type,[6] (b) B-type,[5] and (c) V-type amylose.[17] In the *c*-axis projections, the "UP" means the reducing end of the helix is running up, while the "DOWN" means the reducing end of the helices is running down. Dashed quadrilaterals represent unit cells. Blue dots stand for water molecules. (d) Three possible conformations of the hydroxymethyl group: *gg*, *gt*, and *tg*. The *t* and *g* characters stand for trans and gauche conformations, respectively. The first italic character designates the torsion angle between O5 and O6 (O5−C5−C6−O6), and the second italic character designates the torsion angle between C4 and O6 (C4−C5−C6−O6). The hydrogen atoms in a−c are omitted.

maltotriosyl repeating unit, and the packing of adjacent double helices has a translation by $c/2$ in the unit cell.[6] The B type has a maltosyl repeating unit, and adjacent double helices are packed without translation with respect to the *c*-axis.[7] The differences in the repeating unit for A and B structures were also reflected as the triplet and doublet C1 peak in the ^{13}C NMR spectra, respectively.[9,10]

When complexed with guest molecules, amylose crystallizes into the so-called "V-type" structure. There are a number of V subtypes. In the presence of small guest molecules, e.g., iodine[11] and fatty acids,[12] amylose forms 6-fold left-handed single helices packed in an antiparallel arrangement, which is also called V_6 as shown in Figure 1c.[13,14] The amylose single helix has a hydrophilic outer surface and a hydrophobic inner

dx.doi.org/10.1021/jp411130n | J. Phys. Chem. B 2014, 118, 1775−1783

channel that accommodates the guest molecules (intrahelical association). Crystals of such intrahelical inclusion complexes can be in the form of V-hydrate (V_h) or V-anhydrous (V_a). The V_h has an hexagonal unit cell with parameters $a = b = 13.65$ Å, $c = 8.05$ Å.[15] Upon losing water from within the unit cell, the V_h form can shrink to V_a, which has an orthorhombic unit cell structure with dimensions of approximately $a = 13.0$ Å, $b = 23.0$ Å, $c = 8.05$ Å.[16−18] Molecules bulkier than linear alcohols, such as *tert*-butyl alcohol[19] and 1-naphthol,[20,21] are able to induce 7- and 8-fold amylose helices, respectively. In the current study we focus on the V_6 subtype.

The polymorphic structures of starch have been extensively studied using X-ray diffraction (XRD),[4] electron diffraction,[22] nuclear magnetic resonance (NMR),[9,23] and to some extent Fourier-transform infrared (FTIR)[24] and Raman spectroscopies.[25] XRD and electron diffraction have been the primary techniques employed to construct the structural models that are the foundation of our current knowledge of the crystalline starch structure. However, there remain uncertainties especially regarding the B polymorph, because the proposed structural models are based on data with limited accuracies. The main limitation stems from the fact that amylose single crystals, especially of the B-type, cannot be grown large enough for full, assumption-free refinement of the XRD data. Therefore, in most cases, axially oriented polycrystalline fibers were analyzed.[26] The diffraction patterns of the aligned fibers contain far fewer reflections (clearly distinguishable ones are typically less than 40) than the number of atomic coordinates in the unit cell.[26] Typical XRD analyses of aligned amylose crystals yield structural refinement factor *R*-values of around 0.2, which are 1 order of magnitude larger than typical *R*-values reported for single-crystal protein XRD analyses. Therefore, techniques that could provide complementary information would contribute greatly to our understanding of the polymorphic structures of starch.

Sum-frequency-generation (SFG) spectroscopy is a nonlinear optical technique that can be used to determine molecular structures in noncentrosymmetric materials. In vibrational SFG spectroscopy, two high intensity laser pulses are irradiated simultaneously on the sample; typically, one is in the infrared frequency region (ω_{IR}) and the other in the visible frequency region (ω_{VIS}). Under certain conditions, a sum-frequency pulse ($\omega_{SFG} = \omega_{IR} + \omega_{VIS}$) can be generated and emitted by the sample. The output intensity of the sum-frequency pulse can be expressed as:

$$I(\omega_{SFG}) \propto |\chi_{eff}^{(2)}|^2 I(\omega_{VIS}) I(\omega_{IR}) \quad (1)$$

where $I(\omega_{VIS})$ and $I(\omega_{IR})$ are the intensities of the visible and infrared laser pulses and $\chi_{eff}^{(2)}$ is the second-order effective nonlinear susceptibility:

$$\chi_{eff}^{(2)} = \frac{N \sum_{\alpha,\beta,\gamma} \langle M_{\alpha\beta} A_\gamma \rangle}{\varepsilon_o(\omega_{IR} - \omega_q - i\Gamma)} \quad (2)$$

where N is the number density, ε_o is the dielectric constant of vacuum, $\langle M_{\alpha\beta} A_\gamma \rangle$ is the angle-average of the product of the Raman and infrared tensors of vibration modes, ω_q is the frequency of a vibration mode, and Γ is a damping constant. According to eq 2, as the frequency of the input tunable IR beam (ω_{IR}) approaches ω_q of the sample, the SFG signals are resonantly enhanced. The $\chi_{eff}^{(2)}$ term is zero for molecules in centrosymmetric or random media. It can have nonzero components for molecules or functional groups arranged without centrosymmetry.[27]

The nonlinear optical activity of plant polysaccharides is well-known,[28] but only recently has SFG been applied to investigate native cellulose[29,30] and starch.[31] The noncentrosymmetric requirement for SFG allows the identification of cellulose polymorphs which have slightly different glucan chain packing from one another. On the basis of the SFG spectral features, the chain orientation and the conformation (*tg* or *gt*) of the exocyclic $C6H_2OH$ group can be determined in each cellulose polymorph.[32] For example, cellulose I and II are both linear (1→4)-linked β-glucopyranoses but differ in chain polarity. Cellulose I has parallel chains (reducing ends pointing the same direction) and cellulose II has antiparallel chains in the crystal unit cell. Because the dipoles of the OH groups in antiparallel chains are canceled by symmetry, no SFG signals arise from the hydrogen bonding in cellulose II; in contrast, the OH groups in cellulose I give strong SFG signals. Similarly, it is expected that the noncentrosymmetric requirement of the SFG process will influence the vibration peak intensities of amylose polymorphs and could be used to distinguish the symmetry of each crystalline polymorph.

Several studies have reported the detection of starch using SFG or SHG (second harmonic generation).[30,33−36] By using commercial amylose and amylopectin samples as references, these previous studies noticed that SFG was insensitive to amylose and thus suggested that the signal generation from starch arose from amylopectin instead of amylose. In these previous studies, however, the polymorphism of amylose, amylopectin, and starch was not taken into account. The insensitivity of SFG to amylose may have resulted from the fact that both the commercial amylose and amylose in native starch are largely amorphous.[37] Amylose and amylopectin may exist in different polymorphs described in Figure 1, but no SFG studies have investigated the differences between them, which may provide further insights into the basic structural unit in each crystalline polymorph.

In the present study, we employed the noncentrosymmetry requirement of SFG to distinguish and understand polymorphic crystalline structures of starch. The SFG spectra of high-crystallinity polymorph samples are consistent with the structural models with the antiparallel packing of single helices for V-type and the parallel packing of double helices for A- and B-types. Analyzing 12 native starch samples revealed that there may be conformational difference in the hydroxymethyl groups of A- and B-types, though current models suggests that they are the same. In addition, cyclodextrin (CD)−guest inclusion complexes, analogous to the amylose inclusion complexes, were characterized. With the inclusion guest molecules, the discrete cyclodextrin molecules form more regularly packed crystals than polydisperse amylose and thus are used to compare with the V-amylose SFG spectra. The cyclodextrin−guest inclusion complexes confirmed the SFG signal cancelation when the functional groups are arranged symmetrically.

EXPERIMENTAL SECTION

Materials. Mung bean starch was purchased from a local market and purified from sugars by suspension in water three times followed by centrifugation and drying. High amylose starches (Gelose 80, Hylon VII, and Hylon V), corn starch (Melojel), and waxy maize starch (Amioca) were kindly provided by Ingredion Incorporated (Bridgewater, NJ). Arrowroot starch was provided by Penzeys Spices Company

dx.doi.org/10.1021/jp411130n | J. Phys. Chem. B 2014, 118, 1775−1783

(Wauwatosa, WI). Wheat starch was provided by Archer Daniels Midland Company (Decatur, IL). Amaranth starch was obtained from Nu-World Amaranth, Inc. (Dyersville, IA). Pea starch (Nastar) was provided by Cosucra Groupe Warcoing (Warcoing, Belgium). Tapioca starch was purchased from Thai Food Fish Brand (Thailand). Potato starch, rice starch, potato amylose (essentially free from amylopectin), and iodine were purchased from Sigma-Aldrich, Inc. (St. Louis, MO). α- and β-CD were obtained from American Maize-Products Company (Stamford, CT). Ethanol (200 proof), dimethyl sulfoxide (DMSO), *tert*-butyl alcohol (TBA), potassium iodide (KI), and hydrochloric acid (HCl, 12 N) were obtained from VWR International (Radnor, PA). Palmitic acid (PA) was obtained from Eastman Kodak Company (Rochester, NY).

Starch Sample Preparation. Native starches, including pea starch and Hylon VII starch, were subject to acid hydrolysis. In detail, starch (2%, w/v) was dispersed in 2.2 N HCl and incubated at 40 °C for 1 to 5 days. The dispersion was stirred for 2 min every day. The acid-hydrolyzed starches were recovered by centrifugation (2000*g*, 10 min), washed twice with 50% (v/v) aqueous ethanol solution, and then washed with 100% ethanol. After drying, the starches were annealed in 50% (v/v) aqueous ethanol solution at 110 °C. The annealed starches were washed with 100% ethanol and finally dried.

Amylose/palmitic acid and CD/palmitic acid inclusion complexes were prepared by following the DMSO method of starch−guest inclusion complex preparation.[3] In detail, 500 mg of amylose or CD was dissolved in 10 mL of 95% (v/v) DMSO aqueous solution in a boiling water bath with constant stirring for at least 1 h. Then 1 mL of palmitic acid (50 mg) solution in 95% DMSO preheated at 90 °C was mixed into the amylose solution. The mixed solution was held for 15 min at 90 °C, after which 25 mL of distilled water preheated at 90 °C was rapidly added to the solution with vigorous stirring. Heating was stopped after 15 min, and the sample was allowed to cool for at least 24 h. Inclusion complexes were recovered by centrifugation (2000*g*, 10 min), washed three times with 50% (v/v) aqueous ethanol solution, and then washed with 100% ethanol. The resulting pellet was dried at room temperature in a vacuum desiccator containing Drierite. Dried samples were pulverized into fine powders for further analysis.

V-type amylose with "empty" helical cavities was prepared as follows. Amylose (5%, w/v) was dissolved in 95% (v/v) DMSO aqueous solution in a boiling water bath with constant stirring for at least 1 h. Then the hot amylose dispersion was mixed into 2.5 volumes of ethanol with vigorous stirring. The mixed suspension was then centrifuged (2000*g*, 10 min). The precipitate was washed with 100% ethanol twice and finally dried. The dried powder was annealed in 40% (v/v) aqueous ethanol solution at 70 °C and dried again.

α-CD/KI and β-CD/KI inclusion complexes were prepared according to Noltemeyer and Saenger[38] with some modifications. In detail, a saturated aqueous solution of α-CD (1.5%, w/v) was heated at 70 °C with stirring. A mixture of KI and I_2 with an I^-/I_2 ratio of 1.3/1 was added to achieve an $(I^-/I_2)/\alpha$-CD molar ratio of 5/2. For β-CD, the same concentration was used even though β-CD was less soluble in water than α-CD. The mixed solution was allowed to slowly cool to room temperature and kept still for 2 h. Ethanol (2 times volume of the mixture) was added, and the mixture was centrifuged. The precipitate was dried at room temperature in a vacuum desiccator containing Drierite.

Wide Angle X-ray Diffraction. Wide angle X-ray diffraction (XRD) patterns were obtained with a Rigaku MiniFlex II desktop X-ray diffractometer (Rigaku Americas Corporation, TX). Samples were exposed to Cu Kα radiation (0.154 nm) and continuously scanned between $2\theta = 4°$ and 30° at a scanning rate of 1°/min with a step size of 0.02°. A current of 15 mA and voltage of 30 kV were used for X-ray generation. Data were analyzed with Jade v.8 software (Material Data Inc., Livermore, CA). The area of the amorphous halo generated by Jade software using the cubic spline fit option was subtracted from the total X-ray diffraction area to obtain the crystalline fraction. The degree of crystallinity (%) was then calculated as the crystalline fraction over the total area multiplied by 100.[3]

Sum-Frequency-Generation Spectroscopy. The SFG setup (EKSPLA) used in our laboratory was described in previous studies.[29] A 532 nm laser pulse was generated by frequency doubling of the 1064 nm output from a Nd:YAG laser. An optical parameter generator/amplifier (OPG/OPA) using β-BaB_2O_4 and $AgGaS_2$ crystals was pumped with 532 and 1064 nm laser pulses and generated tunable IR pulses in the wavelength range of 2.3−10 μm with <6 cm^{-1} bandwidth. The incidence angles of visible and IR pulses with respect to surface normal were 60° and 56°, respectively. The incident visible and IR beams were s-polarized and p-polarized, respectively, with respect to the laser incidence plane. The SFG signal was collected in the reflection geometry with no polarization selection. A beam collimator was used to enhance the collection efficiency of the SFG signals. SFG spectra were taken at 4 cm^{-1}/step for the 2700−3050 cm^{-1} region, and 8 cm^{-1}/step in the 3096−3800 cm^{-1}region, with averaging 100 shots/step. Three independent measurements were taken for the acid-hydrolyzed samples and two independent measurements for the twelve native starch samples. Differences between spectra of the same sample were minor.

Chemometric Evaluation. Principal component analyses of XRD and SFG data were carried out using JMP, version 9.0.2 (SAS Institute Inc., Cary NC).

RESULTS AND DISCUSSION

Starch Polymorphs. Starch and amylose samples with enhanced crystallinity were obtained through acid hydrolysis and annealing and were characterized by XRD to determine their crystalline structures (Figure 2). For the pea starch, diffraction peaks characteristic of A-type were observed at $2\theta =$

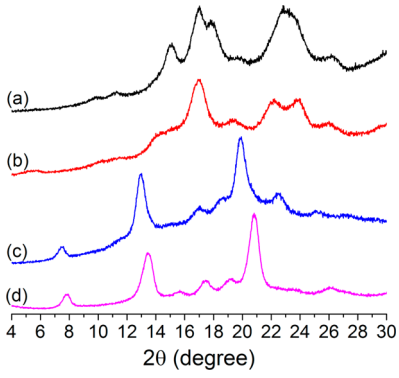

Figure 2. X-ray diffraction patterns of (a) A-type starch (acid-hydrolyzed pea starch), (b) B-type starch (acid-hydrolyzed Hylon VII starch), (c) V_h-type amylose−palmitic acid inclusion complex, and (d) V_a-type amylose without guest.

dx.doi.org/10.1021/jp411130n | J. Phys. Chem. B 2014, 118, 1775−1783

15°, 17°, 17.8°, and 23° (Figure 2a). The Hylon VII starch showed the B-type diffraction pattern at 2θ = 5°, 17°, 19.5°, 22°, and 24° (Figure 2b). A typical signature of B-type starch is the diffraction peak at around 2θ = 5°, which can vary significantly depending on the hydration level of the sample.[39] Because the starch samples were extensively dried in a vacuum desiccator, the 2θ = 5° peak intensity of B-type starches was suppressed. The crystallinities of the pea starch and Hylon VII starch were estimated to be 57% and 52%, respectively. After annealing of the amylose−PA inclusion complex, diffraction peaks at 2θ = 7.5°, 13°, 19.8° and 22.5°, characteristic of the V-type (in particular V_h-type), were observed (Figure 2c). The annealing treatment in aqueous ethanol solution was able to increase the degree of crystallinity of the amylose−PA inclusion complex to ∼43%.[40] V-type amylose without guest inclusion showed XRD peaks at 2θ = 7.8°, 13.4°, and 20.8°, which is characteristic of V_a-type (Figure 2d). The degree of crystallinity was estimated to be 65%, which was higher than most values previously reported for V-type starch.[3]

Figure 3 displays SFG spectra of the crystalline starch and amylose samples shown in Figure 2. It is clearly noticed that the

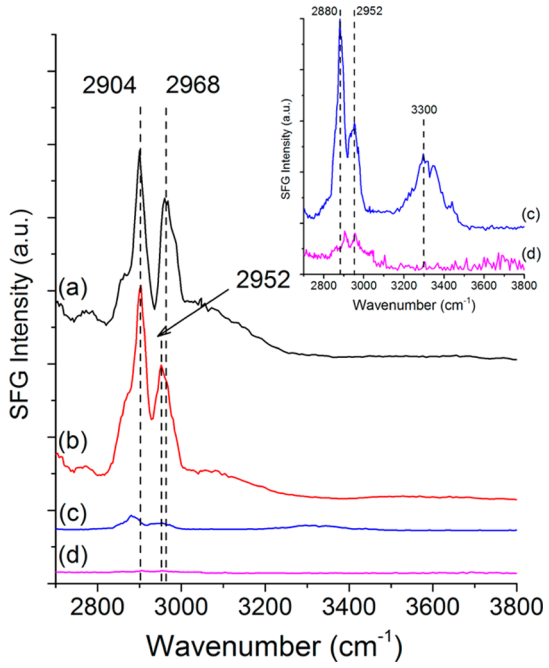

Figure 3. SFG vibrational spectra of (a) A-type starch (acid-hydrolyzed pea starch), (b) B-type starch (acid-hydrolyzed Hylon VII starch), (c) V_h-type amylose−palmitic acid inclusion complex, and (d) V_a-type amylose without guest. Inset shows the magnified spectra of c and d.

SFG intensities of the A- and B-types are strong, while the V-types show very weak SFG signals. The overall weak SFG signal intensity of the V-type amylose samples can be understood with the helix packing direction in the unit cell. The V-amylose unit cell contains two single helices running in the opposite direction (antiparallel packing, Figure 1c). Thus, most of vibration modes in the helix running upward can be symmetry-canceled with those in the helix running downward. This is similar to the intrachain hydrogen-bonded hydroxyl groups in cellulose II which has antiparallel glucan chains in the unit cell.[32] In the A-type starch crystal, the parallel double helices are running in the same direction. Thus, there will be net dipoles of functional groups across the entire crystal. This makes the A-type structure highly efficient for the SFG process. The fact that the SFG signal intensity of the B-type starch is comparable with that of the A-type indicates that the A- and B-type starches must share similar symmetry elements. One possibility is that the B-type starch has the parallel arrangement of helices in the unit cell, similar to the A-type starch. This is consistent with the current models shown in Figure 1a and 1b.

The SFG signal in the O−H stretch region (3000−3800 cm^{-1}) is very weak for all starch samples. The broad and weak hump centered at around 3100 cm^{-1}, which seems stronger in the A-type starch than in the B-type, could be attributed to strongly hydrogen-bonded OH groups (see Discussion below). This is in contrast to the broad OH signal in IR and Raman centered at ∼3280 cm^{-1} and 3390 cm^{-1}, respectively (Supporting Information). The weak O−H SFG signal could imply that water molecules confined in unit cells are symmetrically arranged, resulting in the centrosymmetrical signal cancelation, or they are in disordered or dynamic states, defying strict confinement into the noncentrosymmetric structure.

The center position of these broad OH components in A- and B-type starches are lower than that in cellulose I (∼3320 cm^{-1}),[29] indicating stronger hydrogen bonding interactions. In the current structural models, the distance between hydrogen-bonded oxygen groups (O−H···O) spans from 2.71 to 2.89 Å in cellulose I,[41] 2.61−2.93 Å in A-type starch, and a greater range in B type starch.[4−7] Although not definitive, these results implied that the strongly hydrogen-bonded hydroxyl groups in the starch crystals are more active in SFG than the weakly hydrogen-bonded groups.

In the C−H stretch region (2800−3000 cm^{-1}), the main peaks are observed at ∼2904 cm^{-1} and ∼2968 cm^{-1} for the A-type polymorph and ∼2904 cm^{-1} and ∼2952 cm^{-1} for the B-type polymorph of starch. Comparison with the SFG spectra of cellulose provides some information needed for interpretation of the amylose SFG spectra.[29] The peak at 2904 cm^{-1} corresponding to the stretch vibration of the axial CH (methine) groups in the ring is not observed in cellulose SFG because they are arranged equally at the opposite sides of the linear glucan chain and their dipoles are symmetry-canceled. In contrast, both A- and B-type starches show the axial CH peak at 2904 cm^{-1}. In the helix of starch, regardless of whether single or double, the C1H, C2H, and C4H groups of the glucopyranose ring are pointing outward and the C3H and C5H are pointing inward. All rings are slightly tilted with respect to the helix main axis. In this helical geometry, the axial CH dipoles will add up, forming a net dipole along the helix axis and making them SFG-active when helices are packed in parallel.

The absence of the 2904 cm^{-1} peak for the V-type starch is consistent with the overall symmetry cancelation due to the antiparallel packing of adjacent helices. Similarly, the same symmetry cancelation effect for the methine groups has been reported for crystalline cellulose.[32,42] The V-type starches analyzed in Figure 3 contain fatty acid guest molecules. Thus, it is possible that the peak centered at 2880 cm^{-1} is due to the CH_3 end groups of the guest molecules.[43] When the guest molecule is not present (Figure 3d), the 2880 cm^{-1} peak disappears. However, a weak peak at 2952 cm^{-1} was observed in both Figure 3c (with guest molecules) and Figure 3d (without guest molecules). Thus, this peak appears to be associated with the amylose chain.

dx.doi.org/10.1021/jp411130n | J. Phys. Chem. B 2014, 118, 1775−1783

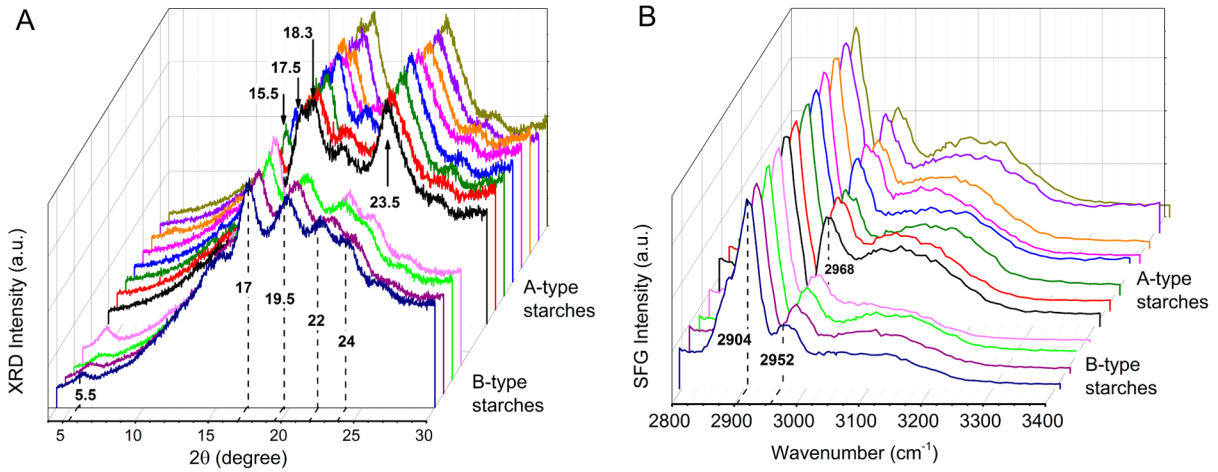

Figure 4. (a) X-ray diffraction patterns and (b) SFG spectra of native starches. SFG spectra were normalized to the 2904 cm^{-1} intensity. The sources of starch are amioca, amaranth, arrowroot, mung bean, rice, tapioca, wheat, melojel, potato, Hylon V, Hylon VII, and Gelose 80 (from top to bottom).

The 2952−2968 cm^{-1} peak can be assigned to the CH_2 stretch vibration of the $C6H_2OH$ group. In the case of cellulose, the $C6H_2OH$ group with the *tg* conformation shows the CH_2 stretch peak at 2944 cm^{-1} (cellulose I) and those with the *gt* conformation show the peak at ∼2960 cm^{-1} (cellulose II and III).[32] If the correlation between the SFG peak position and the $C6H_2OH$ conformation observed for cellulose is applied to the amylose SFG spectra, the data shown in Figure 3 suggest that the exocyclic chain conformations in starch crystals are closer to the *gt* conformation than the *tg* conformation. It is intriguing to note that the CH_2 stretch peak position of the B-type is closer to that of the V-type (2952 cm^{-1}, Figure 3c), rather than the A-type (2968 cm^{-1}, Figure 3a). On the basis of this observation, we speculate that the $C6H_2OH$ conformation in the B-type might be different from that in the A-type; rather it might be close to the V-type.

The current structural models based on XRD analyses suggest that the hydroxymethyl groups of both A- and B-type starches have the *gg* conformation,[5,6] while that of the V-type starch is modeled to take either *gt* or *gg* conformation depending on its complexation status.[26,44,45] NMR studies show that A- and B-type starches have a C6 chemical shift of around 62 ppm, which has been attributed to the *gt* position.[9] However, for the V-type amylose, the C6 shows a wide range of chemical shift across 61−63 ppm, depending on sample preparation and complexation agents.[10,23] Therefore, the assignment to the *gt* or *gg* conformation of the hydroxymethyl groups in A-, B-, and V-type starches is not definitive. The difference in the CH_2 stretch peak positions in the A- and B-type SFG spectra and their similarity between the B-and V-types pose the possibility that the $C6H_2OH$ conformation in A- and B-types might not be the same.

Another key difference between the A- and B-type SFG spectra is the relative intensity ratio of the CH_2 (2952−2968 cm^{-1}) and CH (2904 cm^{-1}) peaks. The CH_2/CH intensity ratio is much lower for the B-type starch than for the A-type (Figure 3a and 3b). This was confirmed by analyzing native starch samples from twelve different sources. Figure 4 compares XRD and SFG data of eight starches in A-type and four starches in B-type. With our experimental setup, all samples in the A-type show a relative CH_2/CH intensity ratio of 0.59 ± 0.03, while the samples in the B-type show a ratio of 0.35 ± 0.01. The difference in the CH_2/CH ratios between native A and B type starches is statistically significant (p-value < 0.001).

The XRD and SFG data were analyzed by principal component analysis (PCA). PCA is a chemometric method which reduces the variation in the entire data set into principle components. The most variant principal components are shown in the Supporting Information. These first principal components (PC1s) accounted for 44% and 67.3% of the total variation in XRD and SFG, respectively. Figure 5 plots the XRD PC1 scores versus the SFG PC1 scores for all native starch samples analyzed. It shows that the variations in XRD and SFG spectra can be grouped into two distinct sets. All A-type starches were clustered in the upper left quadrant, while the B-type starches resided in the lower right quadrant. This PCA analysis result confirmed that the SFG spectra clearly differentiate two polymorphs of starch. The wheat XRD showed a slightly high background in the 2θ = 19.5° region, and the potato XRD gave a peak at 2θ = 22° stronger than the other three B-type starches. So, these XRD PC1 scores seem to deviate most from each group, but their SFG PC1 scores clearly distinguish them into two different groups.

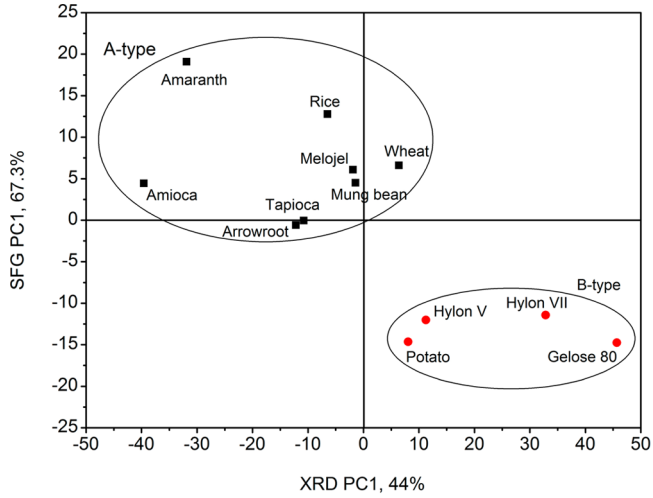

Figure 5. Plot of SFG PC1 scores versus XRD PC1 scores of native starch samples.

dx.doi.org/10.1021/jp411130n | J. Phys. Chem. B 2014, 118, 1775−1783

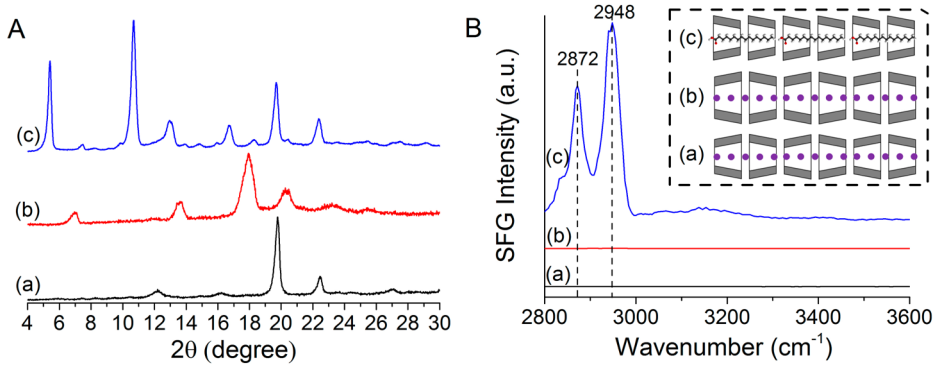

Figure 6. (A) XRD patterns and (B) SFG spectra of (a) α-CD/KI, (b) β-CD/KI, and (c) α-CD/palmitic acid inclusion complexes. Inset shows corresponding models of CD inclusion complexes packing in their crystal structures.

The difference in the CH_2/CH peak intensity ratio found in the SFG analysis implies that there must be structural differences in the helices of the A- and B-type starches. A few hypotheses can be considered to account for this difference. First, although both A- and B-polymorphs are thought to have a parallel double helical structure, it is possible that the hydroxymethyl conformation is different. In the current model, the B-type structure contains many more water molecules between helices than the A-type structure. Thus, there could be many more degrees of freedom in the hydrogen bonds involving the $C6H_2OH$ groups which point toward the interhelical space.[7] The greater degrees of freedom for water molecules in the interhelical space of the B-type structure is also consistent with the weaker OH SFG peak for the B-type, compared to the A-type, as shown in Figures 3 and 4b. Thus, the degree of structural ordering of the $C6H_2OH$ group could be lower in the B-type structure; this could result in a weaker SFG signal for the CH_2 peak of the type-B structure, compared to the A-type structure. The involvement of more water molecules in the interhelix hydrogen bonding network could also alter the angle of the C5−C6−O6 bond; this could bring about a slight shift in the CH_2 stretch peak position (2968 cm^{-1} for type A and 2952 cm^{-1} for type B). The SFG spectral differences between the A- and B-type starches suggest that the $C6H_2OH$ conformation for both A- and B-types may not strictly be *gg* as suggested by XRD.[5−7] NMR also showed that the A- and B-type starches may not exclusively have the *gg* $C6H_2OH$ conformation.[9,10,23] It is possible that the B-polymorph has the *gt* conformation (like V), rather than the *gg* conformation (like A). It is also possible that the V-type inclusion complex samples shown in Figures 2 and 3 might contain a trace amount of B-type.

Although still speculative, one might interpret the differences in the CH_2 peak position and the CH_2/CH relative intensity among A- and B-types to support another hypothesis that the B-type may not be a double-stranded helix. This suggestion arises from the fact that the V-polymorph with antiparallel single helices can be easily converted to the B-polymorph at relatively low temperature (below the melting points) and at low humidity.[46,47] For the V to B transition, Buleon et al. noted that "the double helical conformation, usually proposed for A-type and B-type structures, is questionable. It is unlikely that any drastic conformational change such as defolding/refolding is provoked by such mild treatment as rehydration, unless the helical conformations ascribed to both V_h- and B-types are not very different..."[48] It is not easy to conceive of a simple way to make the transition from antiparallel single helices to parallel double helices in solids with such low mobility (without complete melting and recrystallization).[49]

It should be noted that the transitions between A and B, both of which are considered double-helix structures, are much more difficult. The B to A transition would require more moisture and energy through a so-called heat-moisture treatment.[50,51] This transition could either be a result of the reorganization of the double helices upon dehydration or the recrystallization of melted B double helices. The A to B transition in the solid state was not considered as easy as rehydration but would require a complete dissolution of the A crystallites followed by recrystallization.[51]

Cyclodextrins and Their Inclusion Complexes. Cyclodextrins (CD) are cyclic oligomers of glucose that commonly consist of either six, seven, or eight α-(1,4)-linked D-glucopyranose units, namely α-, β-, and γ-CD, respectively. CDs are able to form inclusion complexes with small molecules and portions of large molecules. The α-, β-, and γ-CD inclusion complexes are homologous with the so-called V_6-, V_7-, and V_8-type amylose inclusion complexes in that they consist of six, seven, and eight glucose residues per turn. However, because they are not polymers, the discrete CD molecules pack differently in a unit cell. Instead of having helical structures, CDs form crystal structures of cage-type,[52] head-to-tail channel-type,[53] head-to-head channel-type,[38] and others depending on the encapsulated guest molecules. We take advantage of the variability of CD structure to understand the SFG peak assignments of both CDs and starches.

CD inclusion complexes were prepared and studied by XRD (Figure 6A). The α-CD inclusion complexes showed a characteristic diffraction peak at $2\theta = 20°$, indicating a similar crystal structure to V_6 amylose (Figure 2c), while the $2\theta = 18°$ peak is characteristic of β-CD inclusion complexes. These peaks were in agreement with the CD inclusion complexes prepared by Takeo and Kuge, who suggested similar packing of V-amylose and coaxially aligned CDs into cylindrical structures.[54] The difference in patterns of the two α-CD inclusion complexes is attributed to the packing of CD molecules, i.e., head-to-head channel-type for α-CD/KI inclusion complex[38] and head-to-tail channel-type when complexed with longer molecules, such as fatty acids.[55]

SFG spectra of α-CD/KI and β-CD/KI showed a very weak signal (Figure 6B). When CDs are packed in a head-to-head manner, all vibration modes of one CD molecule will be symmetry-canceled in SFG by those of the paired one. However, the α-CD/palmitic acid complexes show strong SFG signals, because the CDs are packed in a continuous head-

dx.doi.org/10.1021/jp411130n | J. Phys. Chem. B 2014, 118, 1775−1783

to-tail style. Unlike V-type amylose that contains antiparallel single helices, it seems that the "necklaces" of α-CD/palmitic acid should run in the same direction. The axial CH peak at 2904 cm^{-1} in A- or B-type starch samples was absent in the SFG spectra of α-CD/palmitic acid complex. Because the six glucopyranose units in the α-CD crystal forms a complete circle, instead of a helix, the axial CH dipoles can cancel one another across the CD ring, making them SFG-inactive. Similar to the starch and cellulose cases, the peak at 2948 cm^{-1} could be assigned to the CH_2 stretch vibration of the $C6H_2OH$ group of α-CD. The peak position is rather closer to that of the $C6H_2OH$ group in the *tg* conformation of cellulose Iβ (2944 cm^{-1}), compared with the values observed for the starch samples (2952−2968 cm^{-1}). The conformation of the hydroxymethyl group of α-CD can vary with solvent environment and included guest compound. The *tg* form was not thought to be a favorable conformation,[56] while the hydroxymethyl group may assume *gg*, *gt*, or a mixture of the two conformations depending on guest compounds.[57−59] The exact conformation of the hydroxymethyl group of α-CD would be determined through hydrogen-bonding interactions between the primary alcohols (O6H) and the secondary alcohol groups (O2H and O3H) in the adjacent CD unit. Although no definitive conclusion on the hydroxymethyl group conformation of the α-CD/palmitic acid crystal could be drawn here, SFG provides valuable information on the relationship between the stacking pattern of the CD monomer units in CD inclusion complexes and the symmetry cancelation of SFG signals.

CONCLUSION

Starches of different polymorphic structures were for the first time characterized by SFG vibration spectroscopy. The V-type amylose showed weak SFG signals due to the antiparallel packing of single helices in the crystal unit cell, whereas the A- and B-type starches showed strong peaks at 2904 cm^{-1} and 2952−2968 cm^{-1}, which were assigned to axial CH stretching and CH_2 stretching of the CH_2OH group, respectively. The CH_2/CH intensity ratios of the A- and B-type starches were significantly different. A few hypotheses were proposed to explain this difference. The packing pattern of cyclodextrin molecules also affected the SFG activity of cyclodextrin inclusion compounds. Although the structure of V-type amylose and cyclodextrin inclusion complexes are different, the same symmetry cancelation principle could be used to explain the absence or weakness of some SFG signals. The SFG spectral differences between the A- and B-type starches suggested structural differences among these polymorphs that could not be explained with the current structural models for these polymorphs.

ASSOCIATED CONTENT

Supporting Information

Raman and ATR-FTIR spectra of Hylon V starch, and loading plots for principle component 1 (PC1) of XRD and SFG data. This material is available free of charge via the Internet at http://pubs.acs.org.

AUTHOR INFORMATION

Corresponding Authors

*Tel: +1-814-863-4809; e-mail: shkim@engr.psu.edu.
*Tel: +1-814-863-2960; fax: +1-814-863-6132; e-mail: grz1@psu.edu.

Notes

The authors declare no competing financial interest.

ACKNOWLEDGMENTS

This work was supported by the USDA National Institute for Food and Agriculture, National Competitive Grants Program, National Research Initiative Program 71.1 FY 2007 as grant no. 2007-35503-18392 and by the Center for Lignocellulose Structure and Formation, an Energy Frontier Research Center funded by the U.S. Department of Energy, Office of Science, and Office of Basic Energy Sciences under Award Number DE-SC0001090. The sample preparation and XRD analyses were performed mostly with the support from USDA, and the SFG analyses were performed with DOE support.

REFERENCES

(1) Gallant, D. J.; Bouchet, B.; Baldwin, P. M. Microscopy of Starch: Evidence of a New Level of Granule Organization. *Carbohydr. Polym.* **1997**, *32*, 177−191.
(2) Biliaderis, C. G. Structures and Phase Transitions of Starch Polymers. In *Polysaccharide Association Structures in Food*; Walter, R. H., Ed.; Marcel Dekker: New York, 1998; pp 57−168.
(3) Lay Ma, U. V; Floros, J. D.; Ziegler, G. R. Formation of Inclusion Complexes of Starch with Fatty Acid Esters of Bioactive Compounds. *Carbohydr. Polym.* **2011**, *83*, 1869−1878.
(4) Imberty, A.; Chanzy, H.; Pérez, S.; Bulèon, A.; Tran, V. The Double-Helical Nature of the Crystalline Part of A-Starch. *J. Mol. Biol.* **1988**, *201*, 365−378.
(5) Imberty, A.; Perez, S. A Revisit to the Three-Dimensional Structure of B-Type Starch. *Biopolymers* **1988**, *27*, 1205−1221.
(6) Popov, D.; Buléon, A.; Burghammer, M.; Chanzy, H.; Montesanti, N.; Putaux, J. L.; Potocki-Veronese, G.; Riekel, C. Crystal Structure of A-Amylose: A Revisit from Synchrotron Microdiffraction Analysis of Single Crystals. *Macromolecules* **2009**, *42*, 1167−1174.
(7) Takahashi, Y.; Kumano, T.; Nishikawa, S. Crystal Structure of B-Amylose. *Macromolecules* **2004**, *37*, 6827−6832.
(8) Buleon, A.; Veronese, G.; Putaux, J.-L. Self-Association and Crystallization of Amylose. *Aust. J. Chem.* **2007**, *60*, 706−718.
(9) Veregin, R. P.; Fyfe, C. A.; Marchessault, R. H.; Taylor, M. G. Characterization of the Crystalline A and B Starch Polymorphs and Investigation of Starch Crystallization by High-Resolution Carbon-13 CP/MAS NMR. *Macromolecules* **1986**, *19*, 1030−1034.
(10) Gidley, M. J.; Bociek, S. M. Carbon-13 CP/MAS NMR Studies of Amylose Inclusion Complexes, Cyclodextrins, and the Amorphous Phase of Starch Granules: Relationships between Glycosidic Linkage Conformation and Solid-State Carbon-13 Chemical Shifts. *J. Am. Chem. Soc.* **1988**, *110*, 3820−3829.
(11) Bluhm, T. L.; Zugenmaier, P. Detailed Structure of the V_h-Amylose-Iodine Complex: a Linear Polyiodine Chain. *Carbohydr. Res.* **1981**, *89*, 1−10.
(12) Godet, M. C.; Buleon, A.; Tran, V.; Colonna, P. Structural Features of Fatty Acid-Amylose Complexes. *Carbohydr. Polym.* **1993**, *21*, 91−95.
(13) Rappenecker, G.; Zugenmaier, P. Detailed Refinement of the Crystal Structure of V_h-Amylose. *Carbohydr. Res.* **1981**, *89*, 11−19.
(14) Manley, R. S. J. Chain Folding in Amylose Crystals. *J. Polym. Sci., Part A: Gen. Pap.* **1964**, *2*, 4503−4515.
(15) Brisson, J.; Chanzy, H.; Winter, W. T. The Crystal and Molecular Structure of VH Amylose by Electron Diffraction Analysis. *Int. J. Biol. Macromol.* **1991**, *13*, 31−39.
(16) Rundle, R. E. The Configuration of Starch in the Starch−Iodine Complex. V. Fourier Projections from X-ray Diagrams. *J. Am. Chem. Soc.* **1947**, *69*, 1769−1772.
(17) Winter, W. T.; Sarko, A. Crystal and Molecular Structure of V-Anhydrous Amylose. *Biopolymers* **1974**, *13*, 1447−1460.

(18) Zobel, H. F.; French, A. D.; Hinkle, M. E. X-Ray Diffraction of Oriented Amylose Fibers. II. Structure of V Amyloses. *Biopolymers* **1967**, *5*, 837−845.
(19) Zaslow, B. Characterization of a Second Helical Amylose Modification. *Biopolymers* **1963**, *1*, 165−169.
(20) Cardoso, M. B.; Putaux, J.-L.; Nishiyama, Y.; Helbert, W.; Hÿtch, M.; Silveira, N. P.; Chanzy, H. Single Crystals of V-Amylose Complexed with α-Naphthol. *Biomacromolecules* **2007**, *8*, 1319−1326.
(21) Yamashita, Y.; Ryugo, J.; Monobe, K. An Electron Microscopie Study on Crystals of Amylose V Complexes. *J. Electron Microsc.* **1973**, *22*, 19−26.
(22) Buléon, A.; Delage, M. M.; Brisson, J.; Chanzy, H. Single Crystals of V Amylose Complexed with Isopropanol and Acetone. *Int. J. Biol. Macromol.* **1990**, *12*, 25−33.
(23) Veregin, R. P.; Fyfe, C. A.; Marchessault, R. H. Investigation of the Crystalline "V" Amylose Complexes by High-Resolution Carbon-13 CP/MAS NMR Spectroscopy. *Macromolecules* **1987**, *20*, 3007−3012.
(24) Cael, S. J.; Koenig, J. L.; Blackwell, J. Infrared and Raman Spectroscopy of Carbohydrates. Part III: Raman Spectra of the Polymorphic Forms of Amylose. *Carbohydr. Res.* **1973**, *29*, 123−134.
(25) Godet, M. C.; Tran, V.; Colonna, P.; Buleon, A.; Pezolet, M. Inclusion/Exclusion of Fatty Acids in Amylose Complexes as a Function of the Fatty Acid Chain Length. *Int. J. Biol. Macromol.* **1995**, *17*, 405−408.
(26) Chandrasekaran, R. Molecular Architecture of Polysaccharide Helices in Oriented Fibers. *Adv. Carbohydr. Chem. Biochem.* **1997**, *52*, 311−439.
(27) Boyd, R. W. *Nonlinear Optics*, 3rd ed.; Elsevier: Burlington, MA, 2008.
(28) Reiser, K.; Knoesen, A. Parametric Nonlinearity in Plant Polysaccharides: A New Harvest. *Nonlinear Opt., Quantum Opt.* **2011**, *42*, 203.
(29) Barnette, A. L.; Bradley, L. C.; Veres, B. D.; Schreiner, E. P.; Park, Y. B.; Park, J.; Park, S.; Kim, S. H. Selective Detection of Crystalline Cellulose in Plant Cell Walls with Sum-Frequency-Generation (SFG) Vibration Spectroscopy. *Biomacromolecules* **2011**, *12*, 2434−2439.
(30) Park, Y. B.; Lee, C. M.; Koo, B.-W.; Park, S.; Cosgrove, D. J.; Kim, S. H. Monitoring Meso-Scale Ordering of Cellulose in Intact Plant Cell Walls Using Sum Frequency Generation Spectroscopy. *Plant Physiol.* **2013**, *163*, 907−913.
(31) Miyauchi, Y.; Sano, H.; Mirzutani, G. Selective Observation of Starch in a Water Plant Using Optical Sum-Frequency Microscopy. *J. Opt. Soc. Am. A* **2006**, *23*, 1687−1690.
(32) Lee, C. M.; Mittal, A.; Barnette, A. L.; Kafle, K.; Park, Y. B.; Shin, H.; Johnson, D. K.; Park, S.; Kim, S. H. Cellulose Polymorphism Study with Sum-Frequency-Generation (SFG) Vibration Spectroscopy: Identification of Exocyclic CH2OH Conformation and Chain Orientation. *Cellulose* **2013**, *20*, 991−1000.
(33) Li, H.; Miyauchi, Y.; Tuan, N. A.; Mizutani, G.; Koyano, M. Optical Sum Frequency Generation Image of Rice Grains. *J. Biomater. Nanobiotechnol.* **2012**, *03*, 286−291.
(34) Cox, G.; Moreno, N.; Feijo, J. Second-Harmonic Imaging of Plant Polysaccharides. *J. Biomed. Opt.* **2005**, *10*, 24013.
(35) Zhuo, Z.-Y.; Liao, C.-S.; Huang, C.-H.; Yu, J.-Y.; Tzeng, Y.-Y.; Lo, W.; Dong, C.-Y.; Chui, H.-C.; Huang, Y.-C.; Lai, H.-M.; et al. Second Harmonic Generation Imaging−A New Method for Unraveling Molecular Information of Starch. *J. Struct. Biol.* **2010**, *171*, 88−94.
(36) Mizutani, G.; Koyama, T.; Tomizawa, S.; Sano, H. Distinction Between Some Saccharides in Scattered Optical Sum Frequency Intensity Images. *Spectrochim. Acta, Part A* **2005**, *62*, 845−849.
(37) Jenkins, P. J.; Donald, A. M. The Influence of Amylose on Starch Granule Structure. *Int. J. Biol. Macromol.* **1995**, *17*, 315−321.
(38) Noltemeyer, M.; Saenger, W. Topography of Cyclodextrin Inclusion Complexes. 12. Structural Chemistry of Linear α-Cyclodextrin−Polyiodide Complexes. Models for the Blue Amylose−Iodine Complex. *J. Am. Chem. Soc.* **1980**, *102*, 2710−2722.
(39) Cleven, R.; Van den Berg, C.; Van Der Plas, L. Crystal Structure of Hydrated Potato Starch. *Starch/Stärke* **1978**, *30*, 223−228.
(40) Kong, L.; Ziegler, G. R. Fabrication of Pure Starch Fibers by Electrospinning. *Food Hydrocolloids* **2014**, *36*, 20−25.
(41) Nishiyama, Y.; Langan, P.; Chanzy, H. Crystal Structure and Hydrogen-Bonding System in Cellulose Iβ from Synchrotron X-ray and Neutron Fiber Diffraction. *J. Am. Chem. Soc.* **2002**, *124*, 9074−9082.
(42) Lee, C. M.; Mohamed, N. M. A.; Watts, H. D.; Kubicki, J. D.; Kim, S. H. Sum-Frequency-Generation Vibration Spectroscopy and Density Functional Theory Calculations with Dispersion Corrections (DFT-D2) for Cellulose Iα and Iβ. *J. Phys. Chem. B* **2013**, *117* (22), 6681−6692.
(43) Ye, S.; Noda, H.; Morita, S.; Uosaki, K.; Osawa, M. Surface Molecular Structures of Langmuir−Blodgett Films of Stearic Acid on Solid Substrates Studied by Sum Frequency Generation Spectroscopy. *Langmuir* **2003**, *19*, 2238−2242.
(44) Sarko, A.; Biloski, A. Crystal Structure of the KOH-Amylose Complex. *Carbohydr. Res.* **1980**, *79*, 11−21.
(45) Winter, W. T.; Sarko, A. Crystal and Molecular Structure of the Amylose−DMSO Complex. *Biopolymers* **1974**, *13*, 1461−1482.
(46) Le Bail, P.; Bizot, H.; Pontoire, B.; Buléon, A. Polymorphic Transitions of Amylose-Ethanol Crystalline Complexes Induced by Moisture Exchanges. *Starch/Stärke* **1995**, *47*, 229−232.
(47) Zaslow, B.; Miller, R. L. Hydration of the "V" Amylose Helix. *J. Am. Chem. Soc.* **1961**, *83*, 4378−4381.
(48) Buleon, A.; Le Bail, P.; Colonna, P.; Bizot, H. Phase and Polymorphic Transitions of Starches at Low and Intermediate Water Contents. In *The Properties of Water in Foods: ISOPOW 6 [International Symposium on the Properties of Water]*; Blackie Academic & Professional: London, 1998; pp 160−178.
(49) Le Bail, P.; Buleon, A.; Colonna, P.; Bizot, H. Structural and Polymorphic Transitions of Amylose Induced by Water and Temperature Changes. *Starch Struct. Funct.* **1997**, *51*.
(50) Stute, R. Hydrothermal Modification of Starches: The Difference Between Annealing and Heat/Moisture-Treatment. *Starch/Stärke* **1992**, *44*, 205−214.
(51) Nishiyama, Y.; Putaux, J.; Montesanti, N.; Hazemann, J.-L.; Rochas, C. B→A Allomorphic Transition in Native Starch and Amylose Spherocrystals Monitored by in Situ Synchrotron X-Ray Diffraction. *Biomacromolecules* **2009**, *11*, 76−87.
(52) McMullan, R. K.; Saenger, W.; Fayos, J.; Mootz, D. Topography of Cyclodextrin Inclusion Complexes: Part II. The Iodine-Cyclohexa-Amylose Tetrahydrate Complex; Its Molecular Geometry and Cage-Type Crystal Structure. *Carbohydr. Res.* **1973**, *31*, 211−227.
(53) Hybl, A.; Rundle, R. E.; Williams, D. E. The Crystal and Molecular Structure of the Cyclohexaamylose−Potassium Acetate Complex. *J. Am. Chem. Soc.* **1965**, *87*, 2779−2788.
(54) Takeo, K.; Kuge, T. Complexes of Starchy Materials with Organic Compounds. *Agric. Biol. Chem.* **1969**, *33*, 1174−1180.
(55) Rusa, C. C.; Luca, C.; Tonelli, A. E. Polymer−Cyclodextrin Inclusion Compounds: Toward New Aspects of Their Inclusion Mechanism. *Macromolecules* **2001**, *34*, 1318−1322.
(56) Immel, S.; Brickmann, J.; Lichtenthaler, F. W. Molecular Modeling of Saccharides, 6. Small-Ring Cyclodextrins: Their Geometries and Hydrophobic Topographies. *Eur. J. Org. Chem.* **1995**, *1995*, 929−942.
(57) Harata, K. The Structure of the Cyclodextrin Complex. I. The Crystal and Molecular Structure of the Alpha-Cyclodextrin-p-Iodoaniline Complex. *Bull. Chem. Soc. Jpn.* **1975**, *48*, 2409−2413.
(58) Harata, K. The Structure of the Cyclodextrin Complex. V. Crystal Structures of Alpha-Cyclodextrin Complexes with p-Nitrophenol and p-Hydroxybenzoic Acid. *Bull. Chem. Soc. Jpn.* **1977**, *50*, 1416.
(59) Harata, K.; Uekama, K.; Otagiri, M.; Hirayama, F.; Ogino, H. The Structure of the Cyclodextrin Complex. X. Crystal Structure of Alpha-Cyclodextrin-Benzaldehyde (1:1) Complex Hexahyderate. *Bull. Chem. Soc. Jpn.* **1981**, *54*, 1954−1959.